J. Plasma Physics (2013), vol. 79, part 6, pp. 1049–1056. © Cambridge University Press 2013
doi:10.1017/S0022377813000792

Super rogue waves in ultracold neutral nonextensive plasmas

S. A. EL-TANTAWY[1], N. A. EL-BEDWEHY[2] and W. M. MOSLEM[1]

[1]Department of Physics, Faculty of Science, Port Said University, Port Said 42521, Egypt
(samireltantawy@yahoo.com)
[2]Department of Mathematics, Faculty of Science, Damietta University, New Damietta 34517, Egypt

(Received 23 May 2013; revised 19 June 2013; accepted 20 June 2013; first published online 15 August 2013)

Abstract. The generation of ion-acoustic rogue waves in ultracold neutral plasmas (UNPs) composed of ion fluids and nonextensive electron distribution is investigated. For this purpose, basic equations are reduced to a nonlinear Schrödinger equation (NLSE) using a reductive perturbation technique. The existence region for the rogue waves defined precisely in terms of the critical wavenumber threshold k_c. It is found that increasing the nonextensive parameter q would lead to a decrease of k_c until q approaches to its critical value q_c, then further increase of q beyond q_c enhances k_c; however, k_c shrinks with the increase of the ions effective temperature ratio σ_*. The dependence of the first- and second-order rational solutions profile on the UNP parameters is numerically examined. It is noticed that near to the critical nonextensive parameter q_c, the rogue wave amplitude becomes smaller, but it enhances whenever we stepped away from q_c. However, the enhancement of the temperature ratio σ_* and the wavenumber k reduces the envelope rogue wave amplitudes.

1. Introduction

Over the last few years, a great deal of attention has been devoted to the study of different types of collective processes in ultracold neutral plasmas (UNPs), which are generated in the laboratory by photoionizing laser-cooled atoms near the ionization threshold (Killian and Rolston 2010; Rosenberg and Shukla 2011; Castro et al. 2012; Shukla and Avinash 2012). In most of the laboratory UNP experiments, the electron temperature can be fixed in the range of a few kelvins by tuning the laser frequency just above the ionization threshold. The ion component, which obtains a small momentum during this process, has temperature in the range of milli-kelvin (Shukla and Avinash 2012). Therefore, the UNPs represent a new regime in which the ionic plasma component can be strongly coupled (Shukla 2010; Killian et al. 2012). The clearest distinguishing feature of the UNPs is that the Coulomb interaction energy dominates over the kinetic energy of the ions or, in other words, the ion coupling parameter Γ_i can be quite large, $\Gamma_i \gg 1$ (Shukla 2010), making them strongly coupled systems, similar to dusty plasmas with strongly correlated highly charged dust grains (Shukla and Mamun 2001; Shukla et al. 2003; Ghosh et al. 2011). A theoretical investigation of the ion-acoustic waves (IAWs) in UNPs was published (Shukla 2010) and ion-acoustic shock waves were recently discussed (Shukla et al. 2011). Moreover, the excitation of IAWs in UNPs was reported experimentally (Castro et al. 2010; Killian et al. 2012). Similarly, as in the strongly coupled dusty plasma where the dust-acoustic soliton was created in the laboratory experiments (Samsonov et al. 2002; Sheridan et al. 2008; Thomas et al. 2003), it is expected that many nonlinear waves can also be created in the future UNP experiments (Maucher et al. 2011; McQuillen et al. 2011; Mendonc and Shukla 2011; McQuillen et al. 2013). One of these nonlinear structures is rogue waves (Moslem et al. 2011; Abdelsalam 2013).

Rogue waves, as a special type of solitary waves, have drawn much attention in some fields of nonlinear dispersive media, e.g. in optics, plasma physics, and superfluidity (Solli et al. 2007; Yeom and Eggleton 2007; Stenflo and Marklund 2010; Moslem 2011; Moslem et al. 2011; Shukla and Misra 2012; Abdelsalam 2013). The probability of generate rogue waves strongly increases in a nonlinear stage of modulation instability (MI). So, one possible mathematical model for rogue waves uses rational solutions of the nonlinear Schrödinger equation (NLSE). Recently, the ion-acoustic rogue waves in a multicomponent plasma with a critical concentration of negative ions were investigated experimentally (Bailung et al. 2011; Sharma and Bailung 2013). Chabchoub et al. (2012) found that the super rogue waves (second-order rational solution) may be more real than the first excitations in fields concerned with nonlinear dispersive media, e.g. in optics, plasma physics, and superfluidity. Moreover, Guo et al. (2012) studied the nonlinear propagation of planar ion-acoustic rogue waves in an unmagnetized electron–positron–ion–dust plasma. In addition, they investigate the influence of the plasma parameters on the nonlinear structures

https://doi.org/10.1017/S0022377813000792 Published online by Cambridge University Press

of the first- and second-order ion-acoustic rogue waves within the modulational instability region. This kind of rational solutions could resolve the mystery of rogons observed in multicomponent plasma (Bailung et al. 2011; Sharma and Bailung 2013). Therefore, to the best of our knowledge, the MI of the IAWs in ultracold neutral nonextensive plasmas was not reported before. Thus, the aim of this letter is to investigate the MI and the nonlinear evolution of the first- and second-order rational solutions in the UNPs with nonextensive electron distribution. In Sec. 2, the basic set of fluid equations describing the system is reduced to the NLSE via a reductive perturbation technique. In Sec. 3, the effects of the plasma parameters on the MI and the profile of the first- and second-order rational solutions are discussed. Finally, the results are summarized in Sec. 4.

2. Model equations and derivation of the NLSE

We consider the propagation of a nonlinear ion-acoustic wave packet in a strongly coupled plasma composed of ions fluid and nonextensive electron distribution. The dynamics of the nonlinear IAWs in UNPs is governed by the generalized hydrodynamic equations which, in dimensionless form, can be written as

$$D_t n_i + n_i \partial_x u_i = 0, \tag{1}$$

$$D_\tau \left(n_i D_t u_i + n_i \partial_x \phi + \sigma_* \partial_x n_i\right) = \eta_* \partial_{x,x} u_i, \tag{2}$$

$$\partial_{x,x}\phi = n_e - n_i, \tag{3}$$

where n_e (n_i), u_i, ϕ, x, and t refer to the electron (ion) number density, the ion fluid velocity, the electric potential, space, and time variables, respectively. These variables are normalized, respectively, by the unperturbed ion density $n_i^{(0)}$, the IA speed $C_{si} = (K_B T_e/m_i)^{1/2}$, the thermal potential $K_B T_e/e$, the ion Debye length $\lambda_{Di} = (K_B T_e/4\pi e^2 n_i^{(0)})^{1/2}$, and the inverse ion plasma frequency $\omega_{pi}^{-1} = (4\pi e^2 n_i^{(0)}/m_i)^{-1/2}$, where K_B is the Boltzmann constant and e is the magnitude of the electron charge. Here, $D_\tau = [1+\tau_m \partial_t]$, $D_t = [\partial_t + u_i \partial_x]$, τ_m is the viscoelastic relaxation time (Shukla 2010), and $\eta_* = (\rho + \frac{4}{3}s)/(m_i n_i^{(0)} \omega_{pi} \lambda_{Di}^2)$ is the normalized longitudinal viscosity coefficient, where ρ and s are the transport coefficients of bulk and shear viscosities, respectively, $\sigma_* = (\mu_i T_i + T_*)/T_e$ is the effective temperature ratio, where T_e (T_i) is the electron (ion) temperature, T_* is the effective ion temperature appears due to electrostatic interactions between strongly coupled positive ions (Shukla 2010), and μ_i is the isothermal compressibility factor for ion fluid. There are various approaches for calculating T_*, μ_i, ρ and, s which have been discussed in the literature (see for example Ichimaru et al. 1987; Shukla 2010).

In a collisionless plasma, the most commonly used distribution is the Maxwellian distribution, which indicates that the particles are in thermal equilibrium. However, a number of observations clearly indicate that the presence of fast particles in space and laboratory experiments described by non-Maxwellian distributions (El-Tantawy et al. 2011). One of these distributions is the nonextensive distribution (namely the q-distribution) and it was successfully applied to a number of applications, including plasma wave propagation (Tribeche and Merriche 2011; El-Tantawy et al. 2012; Abdelsalam 2013). The normalized number density of the electrons is expressed as (El-Tantawy et al. 2012)

$$n_e = (1 + (q-1)\,\phi)^{\frac{q+1}{2(q-1)}}. \tag{4}$$

Here, the parameter q denotes the strength of nonextensivity. In the extensive limiting case ($q = 1$), the density (4) reduces to their well-known Maxwell–Boltzmann counterpart. However, for $q < 1$, high energy states are more probable than in the extensive case (i.e. Maxwell–Boltzmann). On the other hand, for $q > 1$ high energy states are less probable than in the extensive case. The nonextensive parameter q was proved to relate to the temperature gradient and the potential energy of the system in terms of the formula $K_B \nabla T + (1-q) Q_s \nabla \phi = 0$, where Q_s is the charge particle. Thus, the deviation of q from unity qualifies the degree of the inhomogeneity of temperature or the deviation from the equilibrium. Therefore, the properties of IAWs derived here are actually those of plasmas in a non-equilibrium stationary state (Liyan and Jiulin 2008). As the UNPs formed in a state that is far from thermal equilibrium, we adopt here a q-nonextensive distribution for electrons, by relying on similar notations as in Liyan and Jiulin 2008 and Tribeche and Merriche 2011 to which the reader is referred for more details.

The MI of the IAWs propagating in the UNPs is investigated using a reductive perturbation technique (derivative expansion method). According to this method, the independent variables are stretched as (Shukla and Misra 2012)

$$\zeta = \varepsilon(x - v_g t) \quad \text{and} \quad \tau = \varepsilon^2 t, \tag{5}$$

where ε is a small (real) parameter and v_g is the group velocity of the envelope IAWs to be determined later. Assuming that all perturbed quantities depend on the fast scale via the phase $\Theta = (kx - \omega t)$, k and ω are real variables representing the fundamental (carrier) wavenumber and frequency, respectively, while the slow scales enter the argument of the lth harmonic amplitude, say, for density as $n_l^{(m)}$. Following this prescription, the dependent variables are expanded as

$$\Psi(x,t) = \Psi^{(0)} + \sum_{m=1}^{\infty} \varepsilon^m \sum_{l=-m}^{m} \Psi_l^{(m)}(\zeta,\tau)\ \exp(il\Theta), \tag{6}$$

where $\Psi_l^{(m)} = [n_{il}^{(m)} \quad u_{il}^{(m)} \quad \phi_l^{(m)}]^T$, $\Psi^{(0)} = [1 \quad 0 \quad 0]^T$. All elements of $\Psi_l^{(m)}$ satisfy the reality condition $\Psi_{-l}^{(m)} = \Psi_l^{*(m)}$, where the asterisk indicates the complex conjugate. We consider the case where the viscosity contribution is small compared to the compressibility

https://doi.org/10.1017/S0022377813000792 Published online by Cambridge University Press

contribution (Veeresha et al. 2010). Hence, the viscous dissipation effects can be neglected by a suitable choice of ordering.

Substituting the expansion (6) with the stretching (5) into (1)–(4) and collecting terms of the same powers of ε, one obtains to the first-order ($m = 1$) and the first harmonic mode ($l = 1$) :

$$n_{i1}^{(1)} = \frac{k}{\omega} u_{i1}^{(1)} = -\gamma \phi_1^{(1)}, \tag{7}$$

where $\gamma = k^2/(k^2\sigma_* - \omega^2)$. Algebraic manipulations of these equations lead to the linear dispersion relation

$$\omega = k\sqrt{\frac{1}{k^2 + \alpha_1} + \sigma_*}, \tag{8}$$

where $\alpha_1 = (1 + q)/2$.

The second-order ($m = 2$) reduced equations with the first harmonic mode $l = 1$ yields

$$n_{i1}^{(2)} = -\gamma \phi_1^{(2)} + i\frac{2\omega}{k^3}\gamma^2 \left(kv_g - \omega\right) \partial_\zeta \phi_1^{(1)}, \tag{9}$$

$$u_{i1}^{(2)} = -\frac{\omega}{k}\gamma \phi_1^{(2)} + i\frac{\gamma^2}{k^4} \left(kv_g - \omega\right) (k^2\sigma_* + \omega^2) \partial_\zeta \phi_1^{(1)}, \tag{10}$$

with the compatibility condition

$$v_g = \frac{\omega}{k}\left[1 - \frac{k^4}{\omega^2\gamma^2}\right] = \partial_k \omega. \tag{11}$$

The second harmonic modes ($m = l = 2$) arising from nonlinear self-interactions of the carrier waves are obtained as

$$Y_2 = A_j \left(\phi_1^{(1)}\right)^2, \tag{12}$$

where $Y_2 = [n_{i2}^{(2)}\ u_{i2}^{(2)}\ \phi_2^{(2)}]^T$ and $A_j = [A_1\ A_2\ A_3]^T$ is given in the Appendix.

The zeroth-harmonic mode also appears due to the self-interaction of the modulated carrier wave. Its expression cannot be determined completely within the second order and we will have to consider the third-order equations ($n = 3$). Thus, the $l = 0$ components of the third-order part of the reduced equations determine the following second-order quantities in the zeroth harmonic,

$$Y_0 = B_j \left|\phi_1^{(1)}\right|^2, \tag{13}$$

where $Y_0 = [n_{i0}^{(2)}\ u_{i0}^{(2)}\ \phi_0^{(2)}]^T$ and $B_j = [B_1\ B_2\ B_3]^T$ is given in the Appendix.

Finally, the third harmonic modes ($m = 3$ and $l = 1$), with the aid of (13), give a system of equations, which can be reduced to the NLSE

$$i\partial_\tau \psi + \frac{1}{2} P \partial_{\zeta,\zeta} \psi + Q|\psi|^2 \psi = 0, \tag{14}$$

where $\phi_1^{(1)} = \psi$ for simplicity. The dispersion coefficient P and the nonlinear coefficient Q are given by the following expressions:

$$P = \frac{C_2}{C_1} = \partial_k v_g \quad \text{and} \quad Q = \frac{C_3}{C_1}, \tag{15}$$

where $C_{1,2,3}$ is given in the Appendix.

3. Modulational instability and rational solutions of the NLSE

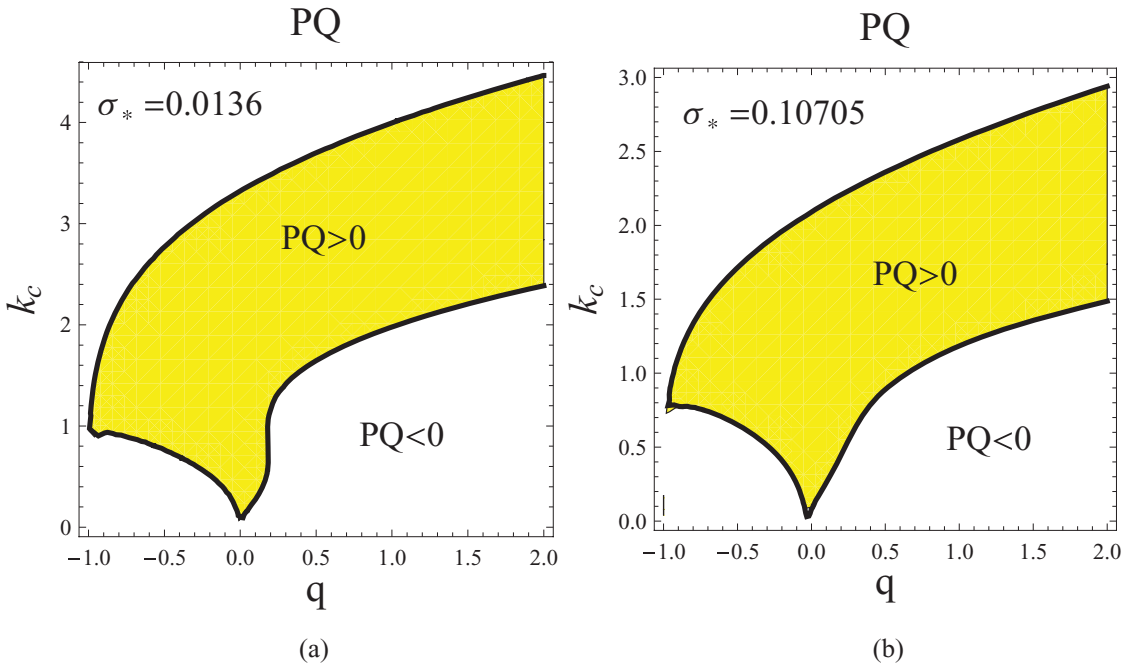
The standard stability analysis of the IAWs consists in linearizing around the monochromatic wave solution of the NLSE (13): $\psi = (\psi_0 + \delta\psi(\xi))\exp(iQ|\hat{\psi}|^2\tau) + c.c.$, where $\xi = \widetilde{k}\zeta - \widetilde{\omega}\tau$ is the modulation phase with the modulation wavenumber $\widetilde{k}(\ll k)$ and frequency $\widetilde{\omega}(\ll \omega)$, and *c.c.* denotes complex conjugate. Furthermore, ψ_0 is the amplitude of the pump carrier wave, $\delta\psi(\ll \psi_0)$ is the small-amplitude perturbation. Assuming that the amplitude perturbation varies as $\delta\psi = (U_0 + iV_0)\exp(i\widetilde{k}\zeta - i\widetilde{\omega}\tau) + c.c.$, where U_0 and V_0 are two real constants. After substituting the latest assumption in (13), one obtains the dispersion relation

$$\widetilde{\omega}^2 = \left(\frac{1}{2}\widetilde{k}^2 P\right)^2 \left(1 - \frac{k_c^2}{\widetilde{k}^2}\right), \tag{16}$$

where $k_c = \sqrt{4Q/P}|\psi_0|$ is the critical value of the modulation wavenumber $\widetilde{k}$. Clearly, if $PQ < 0$, the IAWs are stable in the presence of small perturbation, since $\widetilde{\omega}$ is always a real number. On the other hand, for $PQ > 0$, the MI would set in for $\widetilde{k} < k_c$, i.e. for a wavelength above a threshold $\lambda_c = 2\pi/k_c$ and $\widetilde{\omega}$ becomes imaginary. In the numerical scheme, we have considered the experimental parameter values as in (Castro et al. 2010 and Shukla et al. 2011, where the ions are excited on the primary Sr^+ transition with $Z_i = 1$, $m_i = 88\ m_p$, $T_e = (1\text{–}1000)\,\mathrm{K}$, $T_i = 1\,\mathrm{K}$, $n_0 = 10^{15}\ \mathrm{m}^{-3}$, and the Debye length $\lambda_d \sim 3\text{–}30\ \mu\mathrm{m}$. Our primary aim is to demonstrate the effects of the UNP parameters on the instability of IAWs. Therefore, Fig. 1 shows the polarity region of the product PQ as functions of the wavenumber k of IAWs, the nonextensive parameter q, and the ions effective temperature ratio σ_*. It is seen that there are two critical values of k_c at which the instability sets in. The white regions correspond to $PQ < 0$, and the IAWs are modulationally stable in these regions. As is well known, in the stable region a dark soliton exists. However, in yellow regions with $PQ > 0$, the carrier wave is modulationally 'unstable', and it may either 'collapse', due to (possibly random) external perturbations, or lead to the formation of 'bright' envelope modulated wave packets, i.e., localized envelope 'pulses' confining the carrier wave, while the boundary between the white and yellow regions represents the critical wavenumber threshold k_c for which $PQ = 0$.

Based upon the above finding, we determine in various regimes the critical wavenumber threshold $\widetilde{k}_c$ for which $PQ = 0$, which indicates where the modulational instability sets in. The dependence of k_c for which PQ changes its sign on the plasma parameters q and σ_* is depicted in Fig. 1. It is evident from Fig. 1(a) that for low wavenumber, $k < 1$, increasing q would lead to a decrease of the critical wavenumber k_c until it approaches a certain value $q \equiv q_c \approx 0$; then a further increase in q beyond q_c increases the value of k_c. Furthermore, for high wavenumber, $k > 1$, the k_c

https://doi.org/10.1017/S0022377813000792 Published online by Cambridge University Press



(a) (b)

Figure 1. (Colour online) Product PQ contour is depicted against the critical wavenumber k_c and the nonextensive parameter q with (a) $\sigma_* = 0.0136$ and (b) $\sigma_* = 0.10705$. The yellow (white) color represents the region where the unstable (stable) pulses set in.

enhances with all values of q. It is clear that the ions effective temperature ratio σ_* shrinks k_c (cf. Figs. 1a and b). Also, increasing σ_* would lead to a decrease in the region of instability. Thus, the ion-acoustic envelope will be more structurally unstable against perturbation for higher wavenumbers. This behavior motivates us to the further investigation of rogue wave formation in UNPs.

The NLSE (13) has a rational solution that is located on a nonzero background and localized in both τ and ζ directions. The general convenient way to write each rational solution of (13) is (Ankiewicz et al. 2009, 2010)

$$\psi_j(\zeta,\tilde{\tau}) = \psi_0\left[(-1)^j + \frac{G_j(\zeta,\tilde{\tau}) + i\tilde{\tau}H_j(\zeta,\tilde{\tau})}{F_j(\zeta,\tilde{\tau})}\right]\exp(i\tilde{\tau}), \tag{17}$$

where $\psi_0 = \sqrt{P/Q}$ is the amplitude, $\tilde{\tau} = P\tau$, and j is the order of the solution. Here, $G_j(\zeta,\tilde{\tau})$, $H_j(\zeta,\tilde{\tau})$, and $D_j(\zeta,\tilde{\tau})$ are polynomials in the variables ζ and $\tilde{\tau}$, and $F_j(\zeta,\tilde{\tau})$ has no real zeros. Higher order solutions are progressively more complicated. Therefore, we are concerned explicitly with the cases when $j \leqslant 2$. The solution (17) represents the profile of the rogue wave within the modulational unstable region ($PQ > 0$), which concentrates a significant amount of energy into a relatively small area and, therefore, the rogue waves generate in the present system.

For the first-order rogue wave solution (i.e., $j = 1$), we obtain

$$G_1(\zeta,\tilde{\tau}) = 4,\ H_1(\zeta,\tilde{\tau}) = 8,$$
$$F_1(\zeta,\tilde{\tau}) = 1 + 4\zeta^2 + 4\tilde{\tau}^2.$$

The first-order rogue wave solution is also known as the Peregrine soliton (Peregrine 1983).

For the second-order solution/super rogue wave (i.e., $j = 2$), we have (Akhmediev et al. 2009)

$$G_2(\zeta,\tilde{\tau}) = \frac{3}{8} - 3\zeta^2 - 2\zeta^4 - 9\tilde{\tau}^2 - 10\tilde{\tau}^4 - 12\zeta^2\tilde{\tau}^2,$$

$$H_2(\zeta,\tilde{\tau}) = \frac{15}{4} + 6\zeta^2 - 4\zeta^4 - 2\tilde{\tau}^2 - 4\tilde{\tau}^4 - 8\zeta^2\tilde{\tau}^2,$$

$$F_2(\zeta,\tilde{\tau}) = \frac{1}{8}\left[\frac{3}{4} + 9\zeta^2 + 4\zeta^4 + \frac{16}{3}\zeta^6 + 33\tilde{\tau}^2 + 36\tilde{\tau}^4 + \frac{16}{3}\tilde{\tau}^6 - 24\zeta^2\tilde{\tau}^2 + 16\zeta^4\tilde{\tau}^2 + 16\zeta^2\tilde{\tau}^4\right].$$

Now, we numerically analyze the maximum super rogue wave envelope amplitude $\psi_{2\mathrm{Max}}$ and investigate how the nonextensive parameter q, the ions effective temperature ratio σ_*, and the wavenumber k change its profile. Figure 2(a) shows that for low wavenumber and $q < 0$ the amplitudes of the super rogue waves reduce with the increase of q, but for positive q, the amplitudes enhance with the increase of q. It is noticed that for low wavenumber and near to the k_c curve, the rogue wave amplitude is high and the ion-acoustic rogue wave concentrate a significant amount of energy that makes the pulses taller. However, if we moved away from k_c of the low wavenumber, the energy decreases, which reduces the nonlinearity and the pulses become shorter. Our numerical results exhibit that the nonextensive effect is salient for both positive and negative q. We speculate that this behavior could be explained as follows: for

https://doi.org/10.1017/S0022377813000792 Published online by Cambridge University Press

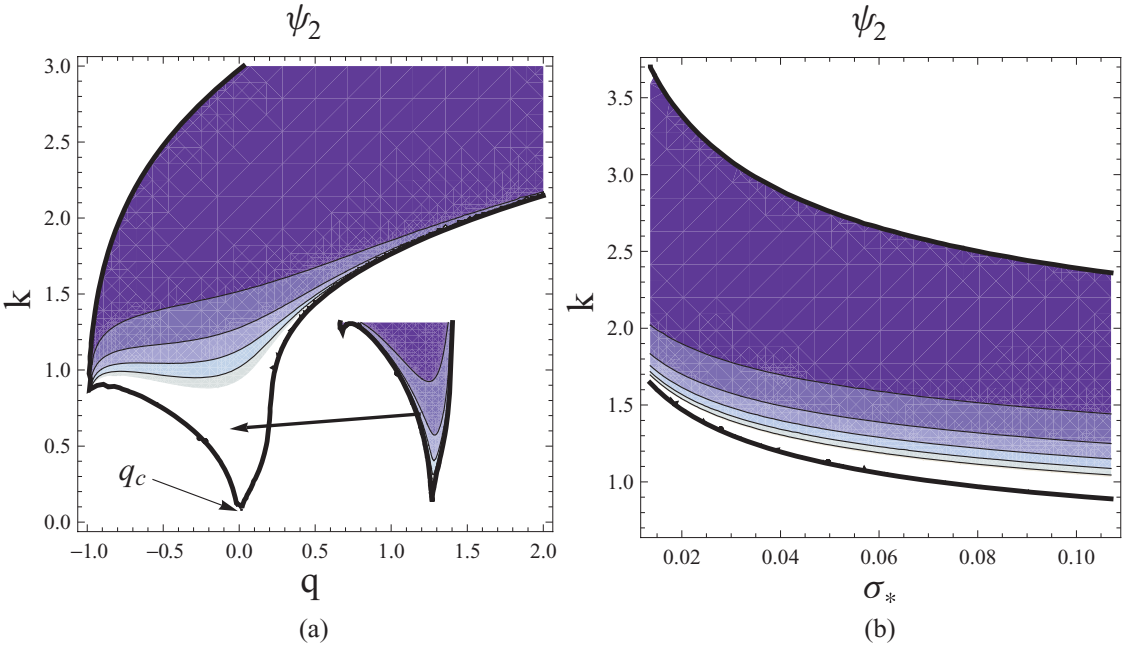


Figure 2. (Colour online) Maximal super rogue wave amplitude $\psi_{2\mathrm{Max}}$ contour is depicted against the wavenumber k and (a) the nonextensive parameter q, with $\sigma_* = 0.02174$ and (b) the ions effective temperature ratio σ_*, with $q = 0.5$. Light-colored regions correspond to high values of $\psi_{2\mathrm{Max}}$. Note that the light color corresponds to the high amplitude region.

certain values of q, the deviation from the equilibrium is strong enough to enhance the nonlinearity and concentrate a significant amount of energy, which makes the pulses taller; however, for other values of q the deviation from the equilibrium is not strong enough to increase the nonlinearity and then the pulses become shorter. Moreover, Fig. 2(b) depicts that increasing the wavenumber k and the ions effective temperature ratio σ_* would lead to the shrinkage of $\psi_{2\mathrm{Max}}$; i.e. increasing k and σ_* reduces the nonlinearity and disperses the energy, which makes the pulses shorter. Hence, the deviation from Maxwellian state would lead to the appearance of new characteristics in the UNPs that should be taken into account during the future experiment. The first-order rational solution ψ_1 has the same qualitative behavior but we did not include its figure here.

Finally, it is interesting to compare the first-order rational solution ψ_1 with the second-order rational solution ψ_2, because Chabchoub et al. (2012) found that the super rogue waves may be more real than the first excitations in fields concerned with nonlinear dispersive media. Figure 3 exhibits the behavior of $|\psi_1|$ and $|\psi_2|$ at a fixed value of q. We found that the super rogue waves have amplitude higher than the first-order case. Furthermore, it is seen that the potential profile of ψ_2 becomes spiky (i.e., taller amplitude and narrower width) than ψ_1.

4. Summary

Summing up, the modulational (in)stability of the envelope IAWs in strongly coupled UNPs composed of ion fluid and nonextensive electrons is investigated. A reductive perturbation technique is used to derive the NLSE, and exact expressions for the dispersion and nonlinearity coefficients were obtained. These have allowed us to study the modulational (in)stability profile of the IAWs in various parameter regimes. The critical wavenumber k_c, which indicates where the modulational instability sets in, has been determined for various regimes. The effects of the nonextensive parameter q and the ions effective temperature ratio σ_* on the critical wavenumber k_c are studied. It is found that for low wavenumber, the critical wavenumber k_c reduces with increasing q in the range $q < 0$, then a further increase of $q > 0$ would lead to the enhancement of the value of k_c. For large wavenumbers, the increase of q would lead to an increase of k_c. Moreover, augmenting the temperature ratio σ_* would lead to reducing k_c for all values of the wavenumber. Within the modulational unstable envelope pulse region, it is possible for a random perturbation of the amplitude to grow and may thus lead to the creation of ion-acoustic rogue waves. The dependence of the first- and second-order rational solutions profiles on our plasma parameters is numerically examined. It is found that the envelope rogue wave amplitudes have complex behavior with the increasing q. However, the enhancement of the temperature ratio σ_* and the wavenumber k reduce the envelope rogue wave amplitudes. Of course, the existence of non-Maxwellian electrons changes the behavior of UNPs. Finally, the present results may be helpful in providing a good fit between the theoretical analysis and real applications in future spatial observations and laboratory plasma experiments in UNPs (Ganshin et al. 2008; McQuillen et al. 2011; Shukla et al. 2011; McQuillen et al. 2013).

https://doi.org/10.1017/S0022377813000792 Published online by Cambridge University Press

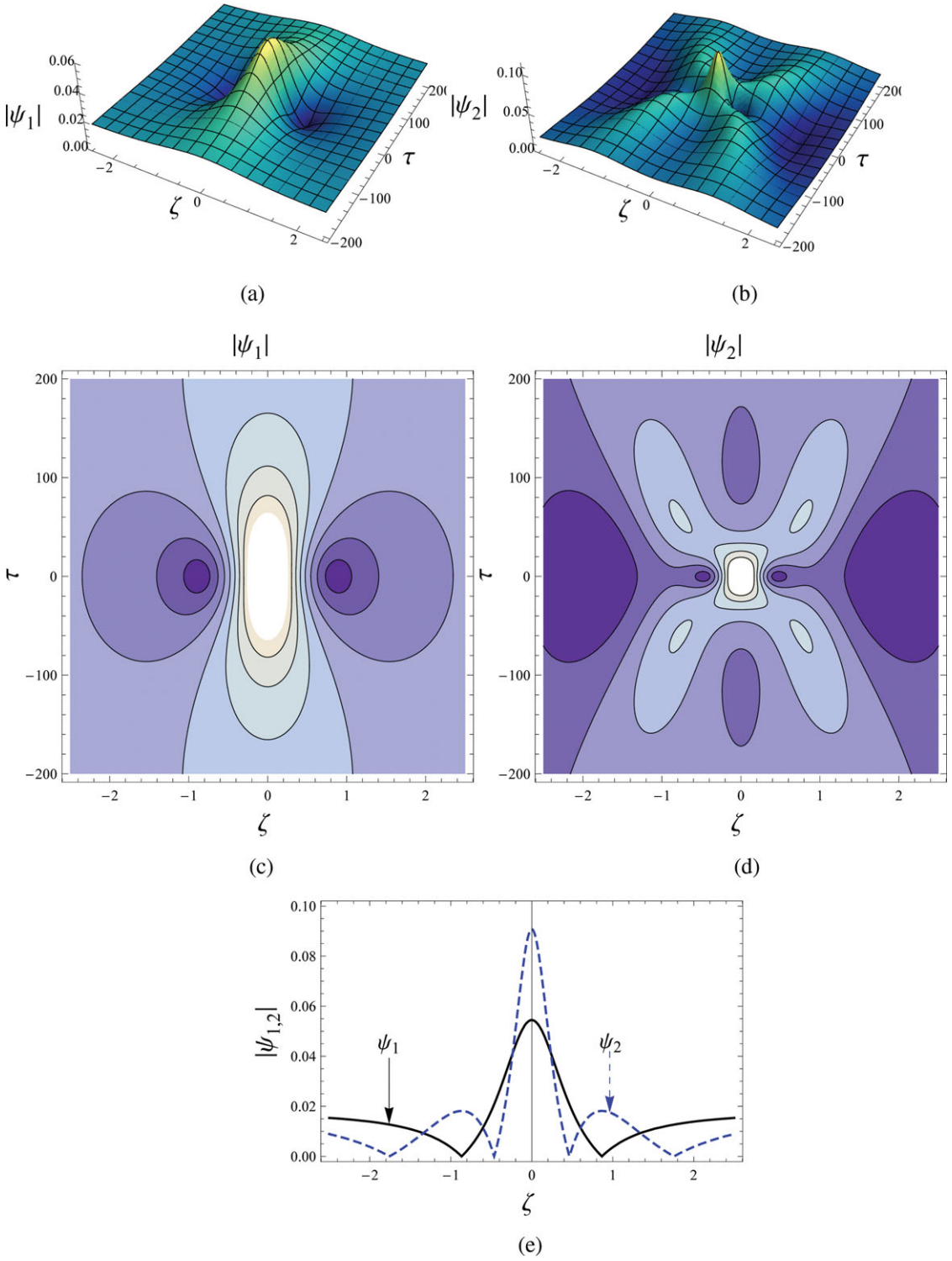


Figure 3. (Colour online) Comparison of the profiles of the first-order rational solution $|\psi_1|$ and the second-order rational solution $|\psi_2|$. (a, b) The absolute value of ψ_1 and ψ_2, respectively; (c, d) contour plot of the latter solutions, respectively; and (e) the solid curve represents the magnitude of $|\psi_1(0,t)|$ and the dashed curve represents the magnitude of $|\psi_2(0,t)|$. Here, $\sigma_* = 0.02174$, $q = 1.5$, and $k = 3$.

Acknowledgements

W. M. Moslem and S. A. El-Tantawy thank the sponsorship provided by the Alexander von Humboldt Foundation (Bonn, Germany) in the framework of the Research Group Linkage Programme funded by the respective Federal Ministry. The authors dedicate this work to the memory of Professor Padma Kant Shukla.

https://doi.org/10.1017/S0022377813000792 Published online by Cambridge University Press

Appendix. Coefficients of Equations (12)–(15)

$$A_1 = \frac{\gamma^2}{W_1}[k^4(4k^2+\widetilde{Z})\sigma_* - k^2(12k^2+2\widetilde{Z}+\alpha_1)\omega^2 + 2\alpha_2\omega^4],$$

$$A_2 = -\frac{\gamma^2\omega}{kW_1}[4k^6\sigma_* + k^4(2+4\omega^2-\widetilde{Z}\sigma_*+2\alpha_1\sigma_*) + k^2(2\widetilde{Z}-\alpha_1)\omega^2 - 2\alpha_2\omega^4],$$

$$A_3 = \frac{\gamma^2}{k^2W_1}[2\alpha_2\omega^6 - 6k^2\alpha_2\omega^4\sigma_* + 3k^4\omega^2(-1+2\alpha_2\sigma_*^2) + k^6(\sigma_* - 2\alpha_2\sigma_*^3)],$$

$$B_1 = \frac{\gamma^2}{W_2}[k^4\widetilde{Z}\sigma_* - k^3\alpha_1 v_g\omega - 2k^2\widetilde{Z}\omega^2 + 2\alpha_2\omega^4],$$

$$B_2 = \frac{\gamma^2}{W_2}[k^4\widetilde{Z}v_g\sigma_* + k^3\omega(-2+\alpha_1(v_g^2-2\sigma_*)) - 2k^2\widetilde{Z}v_g\omega^2 + 2\alpha_2 v_g\omega^4],$$

$$B_3 = \frac{\gamma^2}{W_2}\begin{bmatrix} -k^3v_g\omega + 2\alpha_2\omega^4(v_g^2-\sigma_*) \\ -2k^2\omega^2(1+2\alpha_2(v_g^2-\sigma_*)\sigma_*). \\ +k^4\sigma_*(1+2\alpha_2\sigma_*(v_g^2-\sigma_*)). \end{bmatrix},$$

$$C_1 = -\frac{2\varkappa^2\omega}{k^2},$$

$$C_2 = 2[1 - \frac{\gamma^3}{k^6}(kv_g-\omega)[-3kv_g\omega^2+\omega^3-k^3v_g\sigma_* + 3k^2\omega\sigma_*]],$$

$$C_3 = -3\alpha_3 - 2\alpha_2(A_3+B_3) + \frac{\gamma}{k^2}\begin{bmatrix}\gamma^3\omega^2 + k(2k\gamma A_3 + kB_1 + 2\gamma\omega B_2) \\ +\gamma A_1(\omega^2+k^2\sigma_*)\end{bmatrix},$$

where

$$\widetilde{Z} = (\alpha_1 + 2\alpha_2\sigma_*),$$

$$W_1 = 2k^2[4k^4\sigma_* - \alpha_1\omega^2 + k^2(1+\alpha_1\sigma_* - 4\omega^2)],$$

$$W_2 = k^4[1+\alpha_1(-v_g^2+\sigma_*)],$$

$$\alpha_2 = -\frac{1}{8}(q-3)(q+1),$$

$$\alpha_3 = -\frac{\alpha_2}{6}(3q-5).$$

References

Abdelsalam, U. M. 2013 *J. Plasma Phys* **79**, 287.

Akhmediev, N., Ankiewicz, A. and Soto-Crespo, J. M. 2009 *Phys. Rev.* E **80**, 026601.

Ankiewicz, A., Clarkson, P. A. and Akhmediev, N. 2010 *J. Phys.* A *Math. Theor.* **43**, 122002.

Ankiewicz, A., Devine, N. and Akhmediev, N. 2009 *Phys. Lett.* A **373**, 3997.

Bailung, H., Sharma, S. K. and Nakamura, Y. 2011 *Phys. Rev. Lett.* **107**, 255005.

Castro, J., Bannasch, G., McQuillen, P., Pohl, T. and Killian, T. C. 2012 *AIP Conf. Proc.* **1421**, 31.

Castro, J., McQuillen, P. and Killian, T. C. 2010 *Phys. Rev. Lett.* **105**, 065004.

Chabchoub, A., Hoffmann, N., Onorato, M. and Akhmediev, N. 2012 *Phys. Rev.* X **2**, 011015.

El-Tantawy, S. A., El-Bedwehy, N. A. and Moslem, W. M. 2011 *Phys. Plasmas* **18**, 052113 (and references therein).

El-Tantawy, S. A., Tribeche, M. and Moslem, W. M. 2012 *Phys. Plasmas* **19**, 032104.

Ganshin, A. N., Efimov, V. B., Kolmakov, G. V., Mezhov-Deglin, L. P., and McClintock, P. V. E. 2008 *Phys. Rev. Lett.* **101**, 065303.

Ghosh, S., Gupta, M. R., Chakrabarti, N. and Chaudhuri, M. 2011 *Phys. Rev.* E **83**, 066406.

Guo, S., Mei, L. and Sun, A. 2012 *Ann. Phys.* **332**, 38.

Ichimaru, S., Iyetomi, H. and Tanaka, S. 1987 *Phys. Rep.* **149**, 91.

Killian, T. C., McQuillen, P., O'Neil, T. M. and Castro, J. 2012 *Phys. Plasmas* **19**, 055701.

Killian, T. C. and Rolston, S. L. 2010 *Phys. Today* **63**, 46.

Liyan, L. and Jiulin, D. 2008 *Physica* A **387**, 4821.

Maucher, F., Henkel, N., Saffman, M., Królikowski, W., Skupin, S. and Pohl, T. 2011 *Phys. Rev. Lett.* **106**, 170401.

McQuillen, P., Castro, J. and Killian, T. C. 2011 *J. Phys.* B **44**, 184013.

McQuillen, P., Zhang, X., Strickler, T., Dunning F. B. and Killian, T. C. 2013 *Phys. Rev.* A **87**, 013407.

Mendonc, J. T. and Shukla, P. K. 2011 *Phys. Plasmas* **18**, 042101; Shukla, P. K. and Avinash, K. 2011 *Phys. Rev. Lett.* **107**, 135002.

Moslem, W. M. 2011 *Phys. Plasmas* **18**, 032301; Abdelsalam, U. M., Moslem, W. M., Khater, A. H. and Shukla, P. K. 2011 *Phys. Plasmas* **18**, 092305.

Moslem, W. M., Shukla, P. K. and Eliasson, B. 2011 *Europhys. Lett.* **96**, 25002; Moslem, W. M., Sabry, R., El-Labany, S. K. and Shukla, P. K. 2011 *Phys. Rev.* E **84**, 066402; El-Labanym S. K., Moslem, W. M., El-Bedwehy, N. A., Sabry, R. and Abd El-Razek, H. N. 2011 *Astrophys. Space Sci.* **3**, 923.

Peregrine, D. H. 1983 *J. Aust. Math. Soc.* B **25**, 16.

Rosenberg, M. and Shukla, P. K. 2011 *Phys. Scr.* **83**, 015503.

Samsonov, D., Ivlev, A. V., Quinn, R. A. and Morfill, G. 2002 *Phys. Rev. Lett.* **88**, 095004.

Sharma, S. K. and Bailung, H. 2013 *J. Geophys. Res.* **118**, 919.

Sheridan, T. E., Nosenko, V. and Goree, J. 2008 *Phys. Plasmas* **15**, 073703.

Shukla, P. K. 2010 *Phys. Lett.* A **374**, 3656.

Shukla, P. K. and Avinash, K. 2012 *Plasma Phys. Control. Fusion* **54**, 124030.

Shukla, P. K. and Mamun, A. A. 2001 *IEEE Trans. Plasma Sci.* **29**, 221.

Shukla, P. K. and Misra, A. P. 2012 *Phys. Lett.* A **376**, 2591.

Shukla, P. K., Moslem, W. M., Duha, S. S. and Mamun, A. A. 2011 *Europhys. Lett.* **96**, 65002.

https://doi.org/10.1017/S0022377813000792 Published online by Cambridge University Press

Shukla, P. K., Stenflo, L. and Morfill, G. E. 2003 *IEEE Trans. Plasma Sci.* **31**, 119; Ashrafi, K. S., Mamun, A. A. and Shukla, P. K. 2010 *Europhys. Lett.* **92**, 15004.

Solli, D. R., Ropers, C., Koonath, P. and Jalali, B. 2007 *Nature* **450**, 1054.

Stenflo, L. and Marklund, M. 2010 *J. Plasma Phys.* **76**, 293.

Thomas, H., Morfill, G. E. and Tsytovich, V. N. 2003 *Plasma Phys. Rep.* **29**, 963.

Tribeche, M. and Merriche, A. 2011 *Phys. Plasmas* **18**, 034502.

Veeresha, B. M., Tiwari, S. K., Sen, A., Kaw, P. K. and Das, A. 2010 *Phys. Rev.* E **81**, 036407.

Yeom, D.-I. and Eggleton, B. 2007 *Nature* **450**, 953.

https://doi.org/10.1017/S0022377813000792 Published online by Cambridge University Press